



■ BONE BIOLOGY

Global and local fat effects on bone mass and quality in obesity

INSIGHTS FROM LIPIDOMICS AND 3D IMAGING ASSESSMENT

**X. Dai,
B. Liu,
Q. Hou,
Q. Dai,
D. Wang,
B. Xie,
Y. Sun,
B. Wang**

From Chongqing
Medical University,
Chongqing, China

Aims

The aim of this study was to investigate the global and local impact of fat on bone in obesity by using the diet-induced obese (DIO) mouse model.

Methods

In this study, we generated a diet-induced mouse model of obesity to conduct lipidomic and 3D imaging assessments of bone marrow fat, and evaluated the correlated bone adaptation indices and bone mechanical properties.

Results

Our results indicated that bone mass was reduced and bone mechanical properties were impaired in DIO mice. Lipidomic sequencing and bioinformatic analysis identified 373 differential lipids, 176 of which were upregulated and 197 downregulated. Functional enrichment analysis revealed a significant downregulation of the pathways: fat digestion and absorption (ko04975) and lipolysis regulation in adipocytes (ko04923) in DIO mice, leading to local fat accumulation. The use of 3D imaging confirmed the increase in fat accumulation within the bone marrow cavity of obese mice.

Conclusion

Our study sheds light on the intricate interplay between fat and bone, and provides a non-toxic and non-invasive method for measuring marrow adipose tissue.

Cite this article: *Bone Joint Res* 2023;12(9):580–589.

Keywords: Fat, Bone mass, Marrow adipose tissue, Lipidomics, 3D imaging, Bone quality

Article focus

■ This study addresses the global and local effects of fat on bone in the diet-induced obese (DIO) model.

Key messages

■ Obesity results in impairment of the signalling pathways responsible for fat digestion and absorption, leading to excessive local fat accumulation in the bone marrow cavity, which in turn causes decreased bone mass and impaired bone mechanical properties.

Strengths and limitations

■ We aimed to investigate the mechanisms underlying the adverse effects of fat on bone from a global to a local level.

Non-invasive and non-toxic imaging were employed for the assessment of local fat.

■ A larger sample size is needed for lipidomic sequencing, while the pathways and mechanisms involved require further validation.

■ Furthermore, the measurement of imaging is limited by errors in the threshold range, and reducing these errors ultimately depends on the improvement of imaging technology.

Introduction

With the ageing population, obesity and osteoporosis have become major global health concerns.¹ Osteoporosis is a metabolic disease characterized by reduced bone mass, deteriorating bone microstructure, and bone

Correspondence should be sent to
Bin Wang; email:
bwang@cqmu.edu.cn

doi: 10.1302/2046-3758.129.BJR-
2023-0102.R1

Bone Joint Res 2023;12(9):580–
589.

remodelling imbalance.² Obesity has long been believed to protect the skeleton.³ However, mounting evidence suggests that fat is actually a risk factor for osteoporosis, contributing to bone mass loss.⁴⁻⁶ Morbid obesity is associated with a poorer prognosis and an increased risk of infection in hip and knee arthroplasty (joint arthroplasty surgery).^{7,8}

Localized fat accumulation has an impact on bone metabolism.⁹ Marrow adipose tissue (MAT) can affect bone remodelling through cytokine secretion, fat factor production, and paracrine mechanisms in nearby osteoblasts, leading to a decrease in osteoblast numbers, an increase in adipocytes, and the stimulation of osteoclast activity.¹⁰ Recently, research interest in the link between MAT and bone has grown, primarily due to advances in imaging techniques. Substantial progress has been made in imaging and quantifying MAT in both humans and rodents. Quantitative MRI and MR spectroscopy (MRS) are commonly used in humans to non-invasively monitor MAT development,¹¹⁻¹⁴ whereas histology represents the main tool for evaluating MAT in rodents. MAT quantification can be enhanced by osmium tetroxide staining combined with micro-CT.¹⁵

In this study, we aim to investigate the impact of fat on bone health using lipidomics and 3D imaging. We examined the fat effects on bone health from both a global and local perspective, with the goal of emphasizing the importance of incorporating lipid metabolism therapy in the treatment of bone-related diseases and identifying new therapeutic targets.

Methods

Animals. A total of 22 male C57BL/6 mice, aged eight weeks, were randomly divided into two groups ($n = 11$ each group, three or four each cage), housed under standard conditions (21°C, 55% relative humidity) on a 12-hour light, 12-hour dark cycle, and were fed a normal chow (as control group, CTL) or a high-fat diet with 60 kcal% fat (DIO group) for 12 weeks. The mice were anaesthetized with a pentobarbital sodium solution and euthanized, and the blood was collected for the determination of serum biochemical indicators, which were measured using an automatic biochemical analyzer ($n = 4$ each group). Whole-body composition analysis was performed by dual-energy X-ray absorptiometry (DXA) ($n = 4$ each group). All animal studies were approved by the Institutional Animal Care and Use Committee (IACUC), and an ARRIVE checklist is included in the Supplementary Material to show that the ARRIVE guidelines were adhered to.

Dynamic histomorphometry. Calcein (30 mg/kg) was intraperitoneally injected 14 days and three days before the mice were sacrificed ($n = 3$ each group). Immediately after euthanasia, the left femur was fixed in a 4% paraformaldehyde solution and embedded with methyl methacrylate (MMA). The hard tissue was sectioned with a low-speed precision diamond saw (DTQ-5; WEIYI, China), and the sectioned sample was observed using the Dragonfly 200

multimodal confocal system (Andor, UK). The mineral apposition rate (MAR, $\mu\text{m}/\text{day}$) and bone formation rate (BFR/BS, $\mu\text{m}^3/\mu\text{m}^2/\text{d}$) based on the bone surface were analyzed according to the Nomenclature Committee Guidelines of the American Society for Bone and Mineral Research (ASBMR).¹⁶

Static histomorphometry. The left femur was fixed in 4% paraformaldehyde for 24 hours, decalcified in 14% ethylenediaminetetraacetic acid for four weeks, and embedded in paraffin. A longitudinal section of the femur was stained with haematoxylin and eosin (H&E) or tartrate acid phosphatase (TRAP). The region of interest was the cancellous bone region starting 200 μm below the growth plate and proceeding to 800 μm in the mid-femur.

The quantity of osteoblasts (N.Ob/B.Pm, 1/mm) and the osteoblast surface (Ob.S/B.Pm, %) occupying the trabecular surface in the region of interest were assessed from H&E-stained sections ($n = 4$) and TRAP-stained sections ($n = 4$) using ImageJ software (National Institutes of Health, USA).

Micro-CT and image analysis. The left femur, stripped of soft-tissue, was fixed with flocculent cotton in a centrifuge tube filled with 75% alcohol and scanned with micro-CT (SkyScan1275) ($n = 4$) (Bruker, Belgium). The scan-specific parameter values were as follows: source voltage = 50 kV, source current = 60 μA , image pixel size = 8.00 μm , exposure = 110 ms, and rotation step = 0.20°. The same threshold setting was used for all samples. CTAn in SkyScan was used for all data analysis, and CTVol and CTVox in SkyScan were used for 3D imaging. A detailed description of the quantification of the 3D microarchitecture of the trabecular and cortical bone has been previously reported.¹⁷

Imaging and measurements were performed according to Hounsfield unit (HU) values. All samples, including a tube of water and a tube of empty air, were used for calibration and collected using the same equipment, in the same environment, and with the same parameters. The degree of absorption of water and air served as a reference, that is, HU = 0 for water and HU = -1,000 for air. Image analysis was performed in a region of interest, defined as a region starting from 200 μm under the growth plate and moving 6 mm below. All pixels of adipose tissue and bone within the bone were measured. The calculated thresholds were bone $\geq 3,000$, haematopoietic bone marrow (HBM; red) -200 to 3,000, and MAT (yellow) -200 to -20.

Fat histomorphometry. The area and number of adipocytes, and the proportion of bone marrow adipocytes in the region of interest, were counted in H&E-stained samples using ImageJ software ($n = 4$). The region of interest was selected as the cancellous bone region, starting at 200 μm below the growth plate and proceeding to 800 μm in the mid-femur.

Three-point bending. A three-point bending was performed to complete the fracture in the left tibia ($n = 4$). The left tibia was placed flat on a 6 mm span fixation frame to mitigate the effect of tibial length on mechanical

property measurements. The force and displacement distance data were collected at a loading speed of 0.05 mm/s. The ultimate load (Max force, N, the maximum force in the displacement curve) and stiffness (N/mm, the slope of the linear region of the force-displacement curve) were calculated.

Serum lipidomic sequencing and functional enrichment analysis. The samples ($n = 8$ in each group) were collected after high-speed, low-temperature centrifugation and sent for highly targeted serum lipidome screening (Metware Biotechnology, China). Analyst 1.6.3 (AB Sciex, USA) was used to process mass spectrometric data. Qualitative analysis was performed on the self-established Metware database (MWDB). Differential metabolites were screened by combining the fold change (FC) and the variable importance in projection (VIP) value of the orthogonal projections to latent structures discriminant analysis (OPLS-DA) model ($0.5 \leq FC \leq 2$ and $VIP \geq 1$). A heatmap was drawn using the heatmaply and ComplexHeatmap R packages (R Foundation for Statistical Computing, Austria). Hierarchical cluster analysis (HCA) was used to analyze the metabolite accumulation patterns of the different groups. The differentially expressed metabolites were analyzed based on Kyoto Encyclopedia of Genes and Genomes (KEGG) annotation results. Major enriched pathways were identified based on proportional abundance. The ratio of differential metabolites in a metabolic pathway was calculated as the proportion of enriched differential metabolites to the total number of metabolites in the pathway, expressed as a percentage. To assess the overall changes in KEGG metabolic pathways, the differential abundance (DA) score was employed. This score was calculated by taking the difference between the number of upregulated and downregulated differential metabolites in the pathway, and dividing it by the total number of metabolites annotated to that pathway.

Statistical analysis. All data were analyzed using GraphPad Prism (GraphPad Software, USA) and are presented as means and standard deviations (SDs). The independent-samples *t*-test was used for comparisons between two groups, and a Bland-Altman plot was used to determine the agreement between 3D reconstruction and histomorphometry. Significantly enriched pathways were identified with a hypergeometric test's *p*-value for a given list of metabolites. *P*-values < 0.05 were considered to be statistically significant.

Results

DIO mice display lipid metabolism disorders. DIO mice exhibited increased body weight and percentage of body fat compared to the controls (CTLs) (Figures 1a to 1c). Furthermore, total cholesterol (TC) was significantly increased, while high-density lipoprotein cholesterol (HDL-C) was significantly decreased in DIO animals (Figure 1d).

Obesity reduces the number of osteoblasts but not osteoclasts. The results of bone dynamic histomorphometry experiments showed that the MAR was significantly

reduced in DIO mice, while the BFR/BS was slightly decreased (Figure 2a). The number of osteoblasts (N.Ob/B.Pm) and the percentage of bone surface occupied by osteoblasts (Ob.S/B.Pm) were significantly reduced in DIO mice compared to CTL animals (Figure 2b). No significant differences in the number of osteoclasts (N.Oc/B.Pm) or the percentage of bone surface occupied by osteoclasts (Oc.S/B.Pm) were detected between the two groups (Figure 2c).

Obesity results in impaired bone microarchitecture and bone mechanical properties. Compared with the CTLs, trabecular number (Tb.N) and trabecular bone mass (BV/TV) were slightly decreased in the femur of DIO mice, but the trabecular thickness (Tb.Th) was significantly reduced (Figure 3a). Cortical bone thickness (Ct.Th) and bone mineral density (BMD) also decreased in DIO animals (Figure 3b). Based on the three-point bending test, the maximum load (maximum force) and stiffness of the tibia significantly decreased in DIO mice, compared with CTL (Figure 3c).

Lipidomic sequencing and functional enrichment analysis. A total of 373 lipid metabolites were differentially expressed in DIO mice compared to CTL, 176 of which were upregulated and 197 downregulated (Figure 4a). Differential metabolite clustering analysis showed that the disordered lipids in obese animals were glycerol-phospholipids, glycerol lipids, sphingolipids, fatty acids, sterol lipids, and prenol lipids, with glycerol-phospholipids and glycerol lipids accounting for the largest proportions (Figure 4b). The proportion of differential metabolites in various KEGG metabolic pathways was determined by calculating the ratio of the number of differential metabolites to the total number of metabolites in each enrichment pathway. The results showed that the metabolic pathways (ko01100) had the highest differential metabolite ratio (91.76%), followed by cholesterol metabolism (ko04979) (44.8%), glycerol lipid metabolism (ko00561) (48.75%), glycerophospholipid metabolism (ko00564) (38.35%), sphingolipid metabolism (ko00600) (13.62%), linoleic acid metabolism (ko00591) (15.05%), arachidonic acid metabolism (ko00590) (15.77%), and alpha-ainolenic acid metabolism (ko00592) (14.7%) (Figure 4c). Furthermore, analysis of overall changes in KEGG metabolic pathways revealed significant downregulation in the pathways of fat digestion and absorption (Ko04975) and regulation of lipolysis in adipocytes (Ko04923) (Figure 4d).

MAT expansion. The representative original grayscale image and thresholded image for each tissue are shown in Supplementary Figure a. The results of 3D imaging showed that the fat volume/tissue volume ratio was significantly higher in DIO mice than in CTL; the fat volume showed an increasing but insignificant trend (Figures 5a to 5d). The histomorphometrical results showed that the area and the number of adipocytes, as well as the ratio of fat area to tissue area in region of interest in the DIO mice, increased significantly compared with those of animals in the CTL group (Figures 5e to 5g). The Bland-Altman

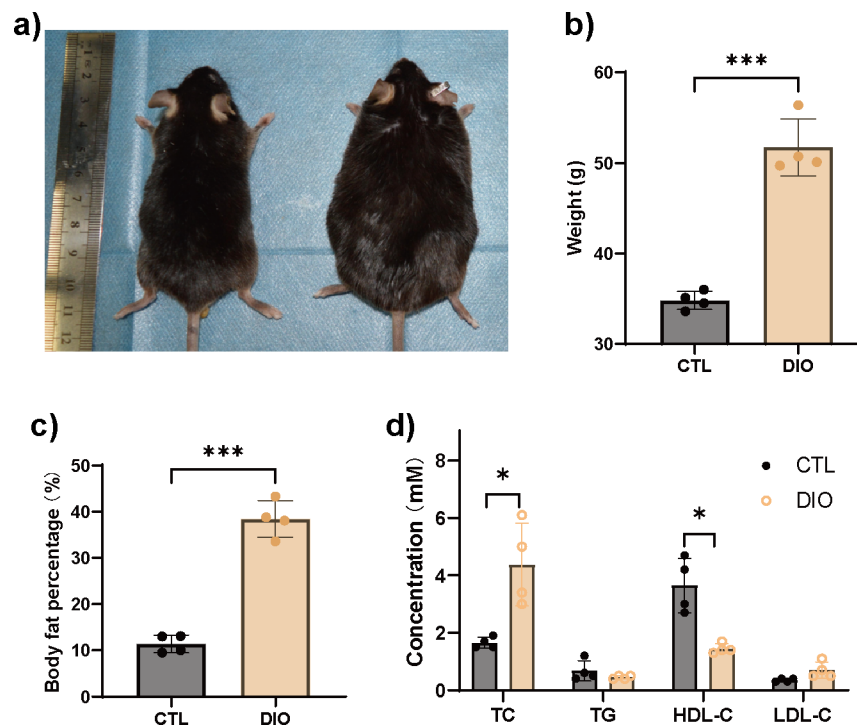


Fig. 1

Diet-induced obese (DIO) mice have metabolism disorders. a) to c) Significantly increased body fat content as determined by dual-energy X-ray absorptiometry (DXA) ($n = 4$). d) Analysis of serum biochemical indicators showed that DIO mice had metabolic disorders. Total cholesterol (TC) was significantly increased, while high-density lipoprotein cholesterol (HDL-C) was significantly decreased ($n = 4$). Data are expressed as means and standard deviations. * $p < 0.05$, *** $p < 0.001$ compared with CTL (independent-samples t -test). CTL, control; LDL-C, low-density lipoprotein cholesterol; TG, triglyceride.

statistical method was used to analyze the consistency between the two methods used to quantify the fat percentage. The Bland-Altman mean difference was 2.530 (limits of agreement: -2.947 to 6.972). The percentage of fat calculated by both methods lay within 2 SDs of the mean percentage difference (Figure 5h).

Discussion

The relationship between fat and bone health has gained increasing importance over recent years. A better understanding of the relationship between fat and bone is conducive to the identification of new drug targets and the exploration of more appropriate therapeutic methods to treat bone diseases while taking lipid metabolism into account. Our study using the DIO mouse model showed that fat slowed bone formation, impaired bone mechanical properties, and reduced bone mass (Figure 3). This is consistent with previous studies indicating that obesity accelerates the differentiation of mesenchymal stem cells into adipocytes at the expense of osteogenic differentiation, ultimately leading to bone loss.¹⁸ Our findings also showed that adipose tissue preferentially affects osteoblast function during bone formation and resorption (Figure 2).

Lipid disorders caused by obesity and redox imbalance due to fat accumulation are considered early triggers in the pathogenesis of metabolic diseases, including those

associated with bone.¹⁹ Lipids play an important role in maintaining cell function and energy storage and are closely related to osteoporosis.²⁰ Previous studies have shown that abnormal lipid metabolism is involved in abnormal adipogenesis of chondrocytes.²¹ Fatty acids, cholesterol, phospholipids, and endogenous metabolites such as prostaglandins exert varying degrees of regulatory effects on bone physiology.²² An in-depth understanding of the role of lipids in bone physiology is essential for investigating pathophysiological changes in bone. In our study, using lipid assays we found that TC was significantly increased and HDL-C was significantly decreased in DIO mice (Figure 1). Apolipoprotein A-1 regulates HDL-C and its absence in *ApoE*^{-/-} mice leads to decreased bone mass due to impaired osteoblast-mediated bone formation and increased osteoclast-mediated bone resorption.²³ Although hypercholesterolaemia can induce osteoporosis,²⁴ physiological levels of TC are necessary for osteogenesis in bone marrow stem cells, and the cholesterol biosynthesis pathway plays a crucial role in their normal development.²⁵ Our study provides additional evidence for the adverse impact of elevated TC and decreased HDL-C levels on bone development; however, the underlying mechanism remains unclear.

A total of 373 differential lipids were identified by serum lipidomic sequencing, 176 of which were significantly upregulated and 197 significantly downregulated.

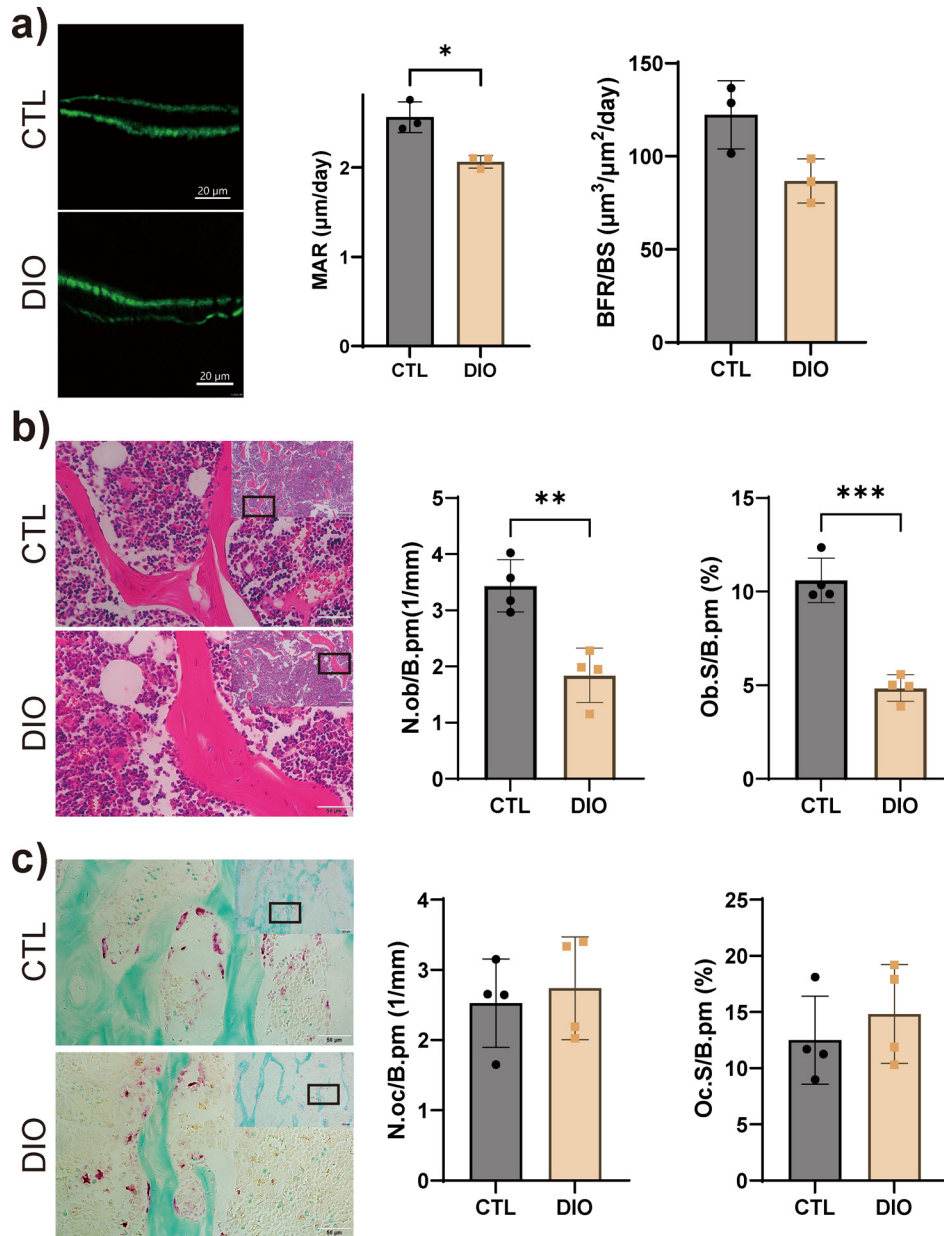


Fig. 2

Obesity negatively regulates bone formation. a) Cancellous bone formation showed a significant decrease in the mineral apposition rate (MAR) as determined using a calcein double-labelling assay ($n = 4$). Magnification: 1,124 \times . b) Osteoblasts were detected by haematoxylin and eosin (H&E) staining and quantified; number of osteoblasts (N.ob/B.pm) and percentage of bone surface occupied by osteoblasts (Ob.S/B.pm) were significantly decreased ($n = 4$). Magnification: 100 \times (top), 400 \times (bottom). c) Osteoclasts were detected by tartrate acid phosphatase (TRAP) staining and quantified; no difference in number of osteoclasts (N.oc/B.pm) or the percentage of bone surface occupied by osteoclasts (Oc.S/B.pm) was detected ($n = 4$). Magnification: 100 \times (top), 400 \times (bottom). Data are expressed as means and standard deviations. * $p < 0.05$, ** $p < 0.01$, *** $p < 0.001$ compared with CTL (independent-samples *t*-test). BFR/BS, bone formation rate; CTL, control; DIO, diet-induced obese.

Cluster analysis revealed that differentially expressed lipids mainly consisted of glycerides and glycerophospholipids (Figures 4a and 4b). Our findings provide additional evidence that disturbances in lipid metabolism can compromise bone health and lead to loss of bone mass. KEGG enrichment analysis indicated that the differentially abundant lipids were enriched in multiple lipid metabolism pathways. Fat digestion and absorption (ko04975) and regulation of lipolysis in adipocytes (ko04923)

pathways were significantly downregulated based on overall metabolic pathway analysis (Figures 4c and 4d). Our study suggested that obesity-induced lipid disorders affect the overall metabolism of lipids, including fat digestion and absorption, which may lead to excessive fat accumulation and, subsequently, impaired bone development.

In this study, we focused on MAT and used non-invasive 3D imaging techniques to investigate the effects

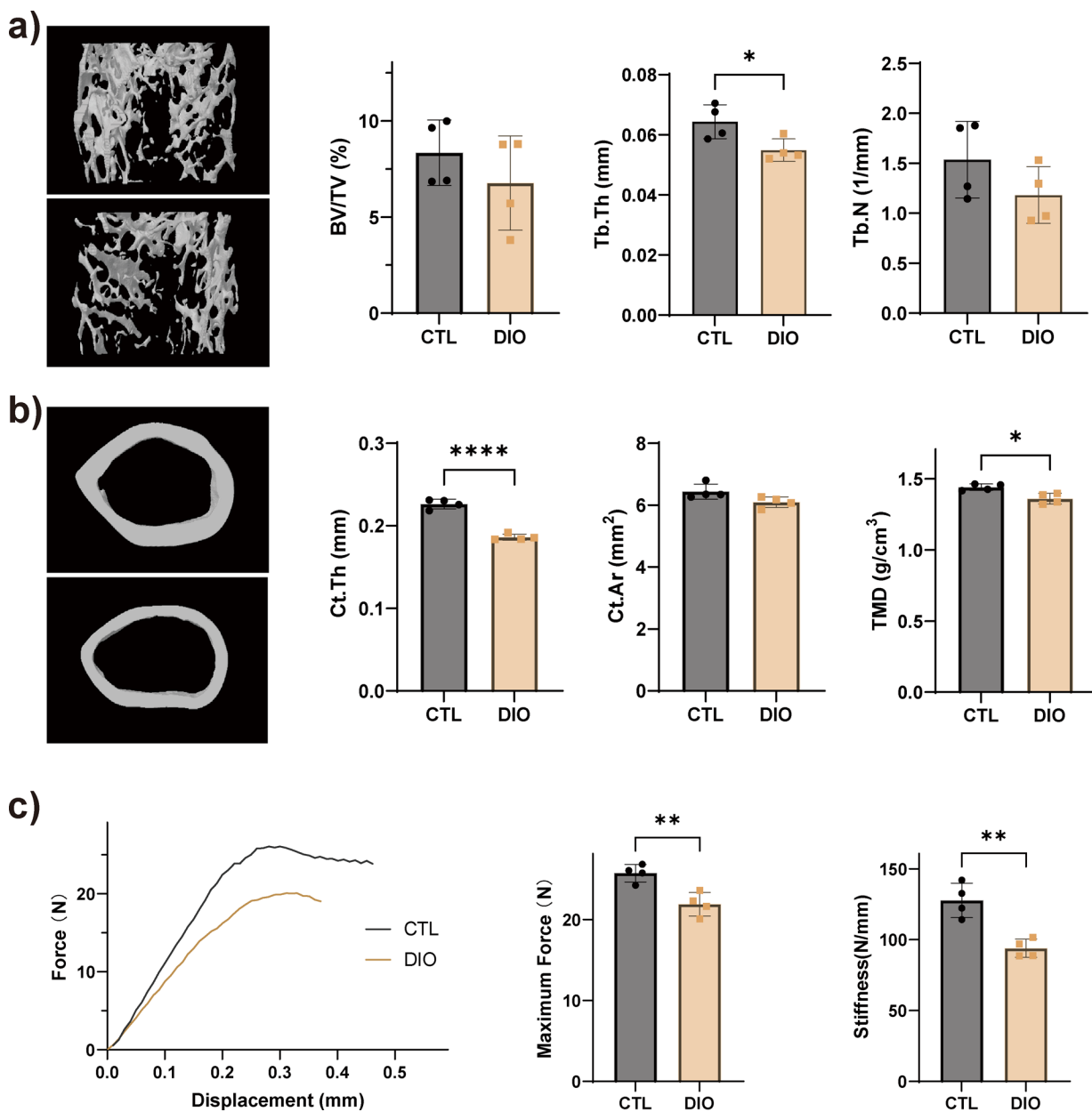


Fig. 3

Obesity reduces bone mass and bone strength. Representative micro-CT (μ CT) reconstruction images and microarchitecture quantification of femoral a) trabecular distal metaphysis and b) mid-diaphyseal cortical bone in control (CTL) and diet-induced obese (DIO) mice. c) The mechanical properties of the tibia were quantified using a three-point bending test; stiffness and maximum force were reduced in DIO animals ($n = 4$). Data are expressed as means and standard deviations. * $p < 0.05$, ** $p < 0.01$, **** $p < 0.0001$ compared with CTL (independent-samples t -test). BV/TV, trabecular bone mass; Ct.Ar, cortical area; Ct.Th, cortical bone thickness; Tb.N, trabecular number; Tb.Th, trabecular thickness; TMD, tissue mineral density.

of fat on bone development. The quality of MAT imaging and quantification have been dependent on the development of novel imaging technologies.²⁶ Micro-CT is a noninvasive imaging technique that uses X-rays with wavelengths between 0.01 nm and 10 nm to calculate HU, which represent tissue attenuation coefficients and are based on air and water normalization points.²⁷ Micro-CT imaging after osmium staining is frequently employed to analyze MAT and other soft-tissues; however, its use has been limited by the severe toxicity of osmium.^{28,29}

The HU of bone, MAT, and HBM tissue was based on validated and previously published protocols.³⁰⁻³² Furthermore, the threshold range was determined according to the tissue thresholds defined based on a previous study.³³ The 3D imaging of bone, MAT, and HBM was performed based on this range, and two trained observers (XD and QD) performed image analysis. The results of 3D imaging and histomorphometric analysis confirmed that the adipose tissue content was increased in the bone marrow cavity in DIO mice, highlighting the potential adverse

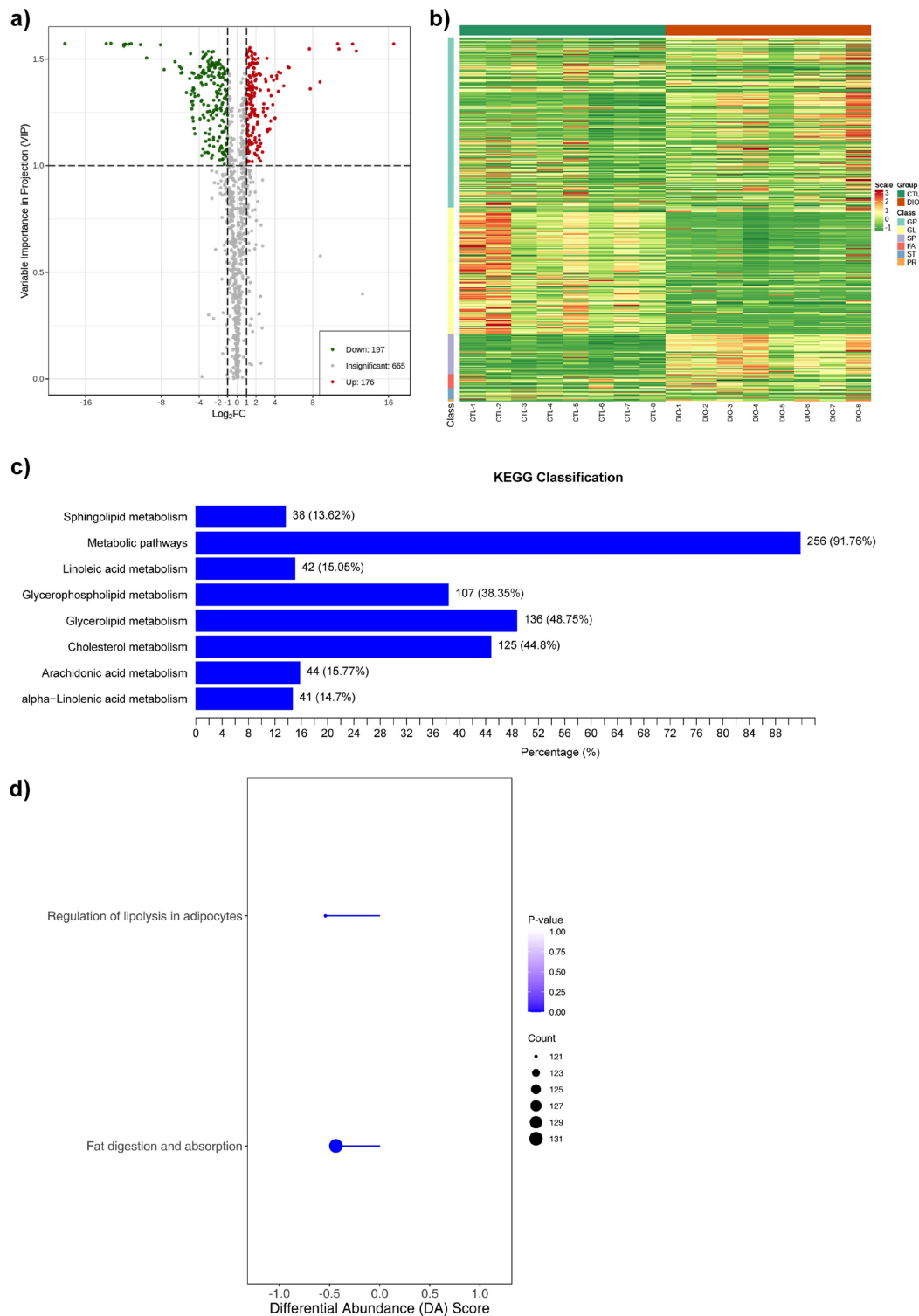


Fig. 4

Lipidomics sequencing and functional enrichment analysis. a) Volcano diagram of differential metabolites (n = 8), with each point representing one metabolite; the green points represent downregulated metabolites (fold change (FC) ≤ 0.5) and the red points represent upregulated metabolites (FC ≥ 2); the x-axis represents the logarithmic value (\log_2FC) of the relative content difference multiple of a metabolite in two groups of samples, and the y-axis represents the variable importance in projection (VIP) value. b) A cluster heatmap of the differential metabolites (n = 8). The x-axis shows sample information and the y-axis shows differential metabolite information. The reported p-value represents the actual value derived from the implementation of the hypergeometric test. c) The main enriched metabolic pathways (n = 8). The y-axis shows the Kyoto Encyclopedia of Genes and Genomes (KEGG) metabolic pathway and the x-axis shows percentage. d) Overall changes in the KEGG metabolic pathways (n = 8). Metabolic pathway names on the y-axis and differential abundance (DA) scores on the x-axis. The hypergeometric test's p-value (< 0.05) indicated significant enrichment of pathways. FA, fatty acyls; GL, glycerolipids; GP, glycerophospholipids; PR, prenol lipids; SP, spingolipids; ST, sterol lipids.

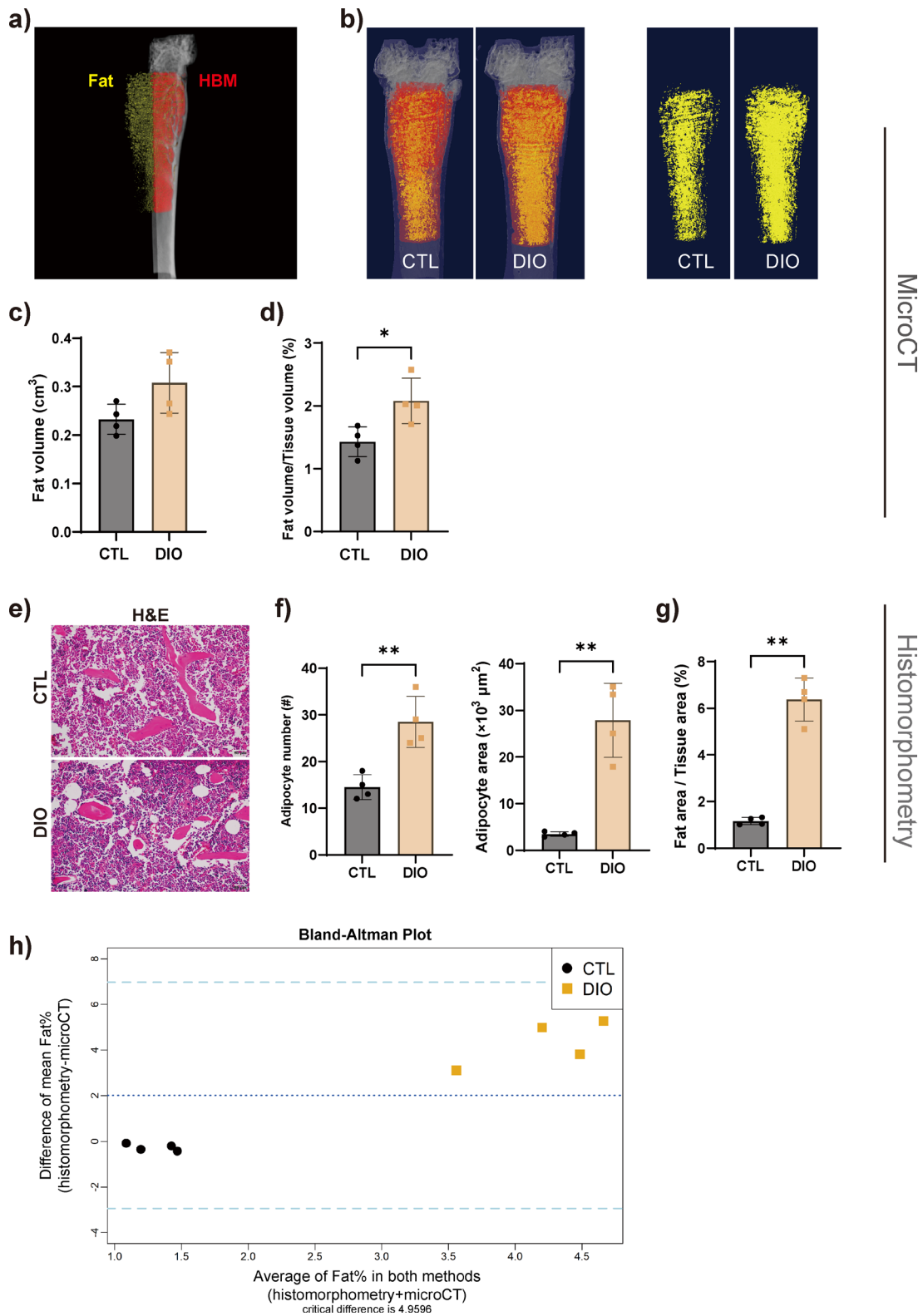


Fig. 5

Marrow adipose tissue (MAT) is increased in diet-induced obese (DIO) mice. a) and b) The MAT content was displayed and quantitatively analyzed by micro-CT 3D imaging (n = 4). c) and d) Results showed that the proportion of fat increased in DIO mice. e) to g) MAT was measured in haematoxylin and eosin (H&E)-stained tissue; the results revealed an increase in the area and number of adipocytes as well as the fat area to tissue area ratio. Magnification in e): 400×. h) Bland-Altman plot analysis showed that the two measurement methods had a certain degree of consistency. The upper and lower dashed lines represent ± 2 standard deviations (SDs), and the middle-dashed line represents the mean (n = 4). Data are expressed as means and SDs. *p < 0.05, **p < 0.01 compared with CTL (independent-samples t-test). CTL, control; HBM, haematopoietic bone marrow.

effects of high-fat diets on bone strength (Figure 5). Indeed, fat accumulation within the bone marrow can negatively impact bone strength.^{34,35} If the specific impact of bone MAT on bone can be determined, targeting the metabolic state of fat instead of osteocytes may represent a novel approach for developing bone-targeted therapies.³⁶ Furthermore, bone MAT is an endocrine organ that plays an active role in regulating systemic metabolism, and this may explain the link between bone fragility and obesity.³⁷ Hence, reasonable measurement of bone MAT is important. Previous studies have extensively used MRI to evaluate bone marrow fat in the general population.^{11–14} Our research primarily focuses on reconstructing CT data, which can effectively quantify bone MAT using HU values in enhanced CT scans. This approach showcases potential clinical applicability. Our study demonstrated that the obesity-related increase in bone MAT led to a decrease in bone mass and compressed the space of bone marrow haematopoietic tissue. Studies on lipid deposition are scarce, and our non-invasive 3D imaging and quantification analysis was helpful in exploring the effect of MAT on bone and identifying potential therapeutic targets for bone-related diseases.

In summary, our results indicate that obesity causes systemic lipid disorders, affecting lipolysis, digestion, and absorption, resulting in local fat excess in the bone marrow, which leads to impaired bone mechanical properties and decreased bone mass. However, the associated mechanisms and pathways require further exploration.

Supplementary material



Figure showing 2D images of original grayscale and thresholded images of bone, fat, and haematopoietic bone marrow in control and diet-induced obese tissue. An ARRIVE checklist is also included to show that the ARRIVE guidelines were adhered to in this study.

References

- Proietto J. Obesity and bone. *F1000Res*. 2020;9:F1000 Faculty Rev-1111.
- Armas LAG, Recker RR. Pathophysiology of osteoporosis: new mechanistic insights. *Endocrinol Metab Clin North Am*. 2012;41(3):475–486.
- Reid IR. Relationships between fat and bone. *Osteoporos Int*. 2008;19(5):595–606.
- Radzki RP, Bieńko M, Filip R, Polak P, Michalik Wolska J. Bone losses in obese, ovariectomized rats appear to be independent from sclerostin-induced inhibition of the Wnt/ β -catenin pathway. *Ann Agric Environ Med*. 2020;27(3):394–400.
- Lu L, Tang M, Li J, et al. Gut microbiota and serum metabolic signatures of high-fat-induced bone loss in mice. *Front Cell Infect Microbiol*. 2021;11:788576.
- Khajuria DK, Soliman M, Elfar JC, et al. Aberrant structure of fibrillar collagen and elevated levels of advanced glycation end products typify delayed fracture healing in the diet-induced obesity mouse model. *Bone*. 2020;137:115436.
- DeMik DE, Carender CN, Glass NA, Brown TS, Callaghan JJ, Bedard NA. Are surgeons still performing primary total knee arthroplasty in the morbidly obese? *Bone Joint J*. 2021;103-B:38–44.
- Crookes PF, Cassidy RS, Machowicz A, et al. Should isolated morbid obesity influence the decision to operate in hip and knee arthroplasty? *Bone Jt Open*. 2021;2(7):515–521.
- Migliaccio S, Greco EA, Fornari R, Donini LM, Di Luigi L, Lenzi A. Skeletal alterations in women affected by obesity. *Aging Clin Exp Res*. 2013;25 Suppl 1:S35–7.
- Kawai M, de Paula FJA, Rosen CJ. New insights into osteoporosis: the bone-fat connection. *J Intern Med*. 2012;272(4):317–329.
- Ruschke S, Pokorney A, Baum T, et al. Measurement of vertebral bone marrow proton density fat fraction in children using quantitative water-fat MRI. *MAGMA*. 2017;30(5):449–460.
- Karampinos DC, Ruschke S, Dieckmeyer M, et al. Quantitative MRI and spectroscopy of bone marrow. *J Magn Reson Imaging*. 2018;47(2):332–353.
- Baum T, Rohrmeier A, Syväri J, et al. Anatomical variation of age-related changes in vertebral bone marrow composition using chemical shift encoding-based water-fat magnetic resonance imaging. *Front Endocrinol*. 2018;9:141.
- Singhal V, Bredella MA. Marrow adipose tissue imaging in humans. *Bone*. 2019;118:69–76.
- Scheller EL, Troiano N, Vanhoutan JN, et al. Use of osmium tetroxide staining with microcomputerized tomography to visualize and quantify bone marrow adipose tissue in vivo. *Methods Enzymol*. 2014;537:123–139.
- Dempster DW, Compston JE, Drezner MK, et al. Standardized nomenclature, symbols, and units for bone histomorphometry: a 2012 update of the report of the ASBMR Histomorphometry Nomenclature Committee. *J Bone Miner Res*. 2013;28(1):2–17.
- Bouxsein ML, Boyd SK, Christiansen BA, Goldberg RE, Jepsen KJ, Müller R. Guidelines for assessment of bone microstructure in rodents using micro-computed tomography. *J Bone Miner Res*. 2010;25(7):1468–1486.
- Infante A, Rodríguez CI. Osteogenesis and aging: lessons from mesenchymal stem cells. *Stem Cell Res Ther*. 2018;9(1):244.
- Furukawa S, Fujita T, Shimabukuro M, et al. Increased oxidative stress in obesity and its impact on metabolic syndrome. *J Clin Invest*. 2004;114(12):1752–1761.
- During A. Osteoporosis: A role for lipids. *Biochimie*. 2020;178:49–55.
- Wang H, Shi Y, He F, et al. GDF11 inhibits abnormal adipogenesis of condylar chondrocytes in temporomandibular joint osteoarthritis. *Bone Joint Res*. 2022;11(7):453–464.
- During A, Penel G, Hardouin P. Understanding the local actions of lipids in bone physiology. *Prog Lipid Res*. 2015;59:126–146.
- Papachristou NI, Blair HC, Kalyvioti ES, et al. Western-type diet differentially modulates osteoblast, osteoclast, and lipoblast differentiation and activation in a background of APOE deficiency. *Lab Invest*. 2018;98(12):1516–1526.
- Zhou Y, Deng T, Zhang H, et al. Hypercholesterolaemia increases the risk of high-turnover osteoporosis in men. *Mol Med Report*. 2019;19:4603–4612.
- Yin W, Li Z, Zhang W. Modulation of bone and marrow niche by cholesterol. *Nutrients*. 2019;11(6):1394.
- Aparisi Gómez MP, Ayuso Benavent C, Simoni P, Aparisi F, Guglielmi G, Bazzocchi A. Fat and bone: the multiperspective analysis of a close relationship. *Quant Imaging Med Surg*. 2020;10(8):1614–1635.
- Hounsfield GN. Computed medical imaging. *Science*. 1980;210(4465):22–28.
- Horowitz MC, Berry R, Holtrup B, et al. Bone marrow adipocytes. *Adipocyte*. 2017;6(3):193–204.
- Lareida A, Beckmann F, Schrott-Fischer A, Glueckert R, Freysinger W, Müller B. High-resolution X-ray tomography of the human inner ear: synchrotron radiation-based study of nerve fibre bundles, membranes and ganglion cells. *J Microsc*. 2009;234(1):95–102.
- Demontiero O, Li W, Thembani E, Duque G. Validation of noninvasive quantification of bone marrow fat volume with microCT in aging rats. *Exp Gerontol*. 2011;46(6):435–440.
- Bani Hassan E, Alderghaffar M, Wauquier F, et al. The effects of dietary fatty acids on bone, hematopoietic marrow and marrow adipose tissue in a murine model of senile osteoporosis. *Aging*. 2019;11(18):7938–7947.
- Demerath EW, Ritter KJ, Couch WA, et al. Validity of a new automated software program for visceral adipose tissue estimation. *Int J Obes (Lond)*. 2007;31(2):285–291.
- Beekman KM, Duque G, Corsi A, Tencerova M, Bisschop PH, Paccou J. Osteoporosis and bone marrow adipose tissue. *Curr Osteoporos Rep*. 2023;21(1):45–55.
- Rosen CJ, Bouxsein ML. Mechanisms of disease: is osteoporosis the obesity of bone? *Nat Clin Pract Rheumatol*. 2006;2(1):35–43.
- Tencerova M, Figeac F, Ditzel N, Taipaleenmäki H, Nielsen TK, Kassem M. High-fat diet-induced obesity promotes expansion of bone marrow adipose tissue and impairs skeletal stem cell functions in mice. *J Bone Miner Res*. 2018;33(6):1154–1165.
- Lecka-Czernik B, Stechschulte LA. Bone and fat: a relationship of different shades. *Arch Biochem Biophys*. 2014;561:124–129.
- Fazeli PK, Horowitz MC, MacDougald OA, et al. Marrow fat and bone—new perspectives. *J Clin Endocrinol Metab*. 2013;98(3):935–945.

Author information:

- X. Dai, MM, Medical Doctoral Student
- B. Wang, PhD, Associate Professor
Department of General Practice, Yongchuan Hospital of Chongqing Medical University, Chongqing, China; Institute of Life Sciences, College of Basic Medicine, Chongqing Medical University, Chongqing, China.
- B. Liu, PhD, Professor, Central Laboratory, Yongchuan Hospital of Chongqing Medical University, Chongqing, China.
- Q. Hou, PhD, Lecturer
- Y. Sun, PhD, Lecturer
Department of Geriatrics, The First Affiliated Hospital of Chongqing Medical University, Chongqing, China.
- Q. Dai, MBBS, Laboratory Technician, Department of Orthopedics, Third Military Medical University Southwest Hospital, Chongqing, China.
- D. Wang, MM, Attending Physician, Department of Stomatology, Third Military Medical University Southwest Hospital, Chongqing, China.
- B. Xie, MM, Chief Physician, Department of General Practice, Yongchuan Hospital of Chongqing Medical University, Chongqing, China.

Author contributions:

- X. Dai: Conceptualization, Data curation, Formal analysis, Visualization, Writing – original draft, Writing – review & editing.
- B. Liu: Conceptualization, Writing – review & editing.
- Q. Hou: Methodology, Writing – review & editing.
- Q. Dai: Visualization, Writing – review & editing.
- D. Wang: Investigation, Writing – review & editing.
- B. Xie: Resources, Writing – review & editing.
- Y. Sun: Funding acquisition, Project administration, Writing – review & editing.
- B. Wang: Conceptualization, Resources, Supervision, Writing – review & editing.

Funding statement:

- The authors disclose receipt of the following financial or material support for the research, authorship, and/or publication of this article: funding from the National Natural Science Foundation of China (81901424), the Natural Science Foundation of Chongqing, China (CSTB2022NSCQ-MSX0110), Postgraduate research innovation project of Chongqing, China (CYB22217), and the Program for Youth Innovation in Future Medicine, Chongqing Medical University (W0046).

ICMJE COI statement:

- The authors declare that they have no conflict of interest regarding the content of this article.

Data sharing:

- The data that support the findings for this study are available to other researchers from the corresponding author upon reasonable request.

Ethical review statement:

- All animal experiments were conducted following the ARRIVE guidelines, and approved by the Institutional Animal Care and Use Committee (IACUC) of Chongqing Medical University.

Open access funding:

- The authors report that they received open access funding for their manuscript from the National Natural Science Foundation of China (81901424), the Natural Science Foundation of Chongqing, China (CSTB2022NSCQ-MSX0110), and the Program for Youth Innovation in Future Medicine, Chongqing Medical University (W0046).

© 2023 Author(s) et al. This is an open-access article distributed under the terms of the Creative Commons Attribution Non-Commercial No Derivatives (CC BY-NC-ND 4.0) licence, which permits the copying and redistribution of the work only, and provided the original author and source are credited. See <https://creativecommons.org/licenses/by-nc-nd/4.0/>